Applied Energy 93 (2012) 733–741

Contents lists available at SciVerse ScienceDirect

Applied Energy

journal homepage: www.elsevier.com/locate/apenergy

# Investigations of the temperature distribution in proton exchange membrane fuel cells

Chi-Young Jung [a], Hyo-Sub Shim [b], Sang-Man Koo [a], Sang-Hwan Lee [c], Sung-Chul Yi [a,*]

[a] Department of Chemical Engineering, Hanyang University, Haengdang-dong, Seongdong-gu, Seoul 133-791, Republic of Korea
[b] Fuel Cell Vehicle Team 1, Hyundai-Kia Motors, Mabuk-dong, Gilheung-gu, Yongin 446-912, Republic of Korea
[c] Department of Mechanical Engineering, Hanyang University, Haengdang-dong, Seongdong-gu, Seoul 133-791, Republic of Korea

ARTICLE INFO

*Article history:*
Received 20 December 2010
Received in revised form 18 July 2011
Accepted 19 August 2011
Available online 4 October 2011

*Keywords:*
PEMFC
Non-isothermal
Agglomerate
Nafion
CFD

ABSTRACT

A two-dimensional, non-isothermal model of a proton exchange membrane fuel cell was implemented to elucidate heat balance through the membrane electrode assembly (MEA). To take local utilization of platinum catalyst into account, the model was presented by considering the formation of agglomerated catalyst structure in the electrodes. To estimate energy balance through the MEA, various modes of heat generation and depletion by reversible/irreversible heat release, ohmic heating and phase change of water were included in the present model. In addition, dual-pathway kinetics, that is a combination of Heyrovsky–Volmer and Tafel–Volmer kinetics, were employed to precisely describe the hydrogen oxidation reaction. The proposed model was validated with experimental cell polarization, resulting in excellent fit. The temperature distribution inside the MEA was analyzed by the model. Consequently, a thorough investigation was made of the relation between membrane thickness and the temperature distribution inside the MEA.



## 1. Introduction

Proton exchange membrane fuel cells (PEMFCs) are very attractive as an alternative power sources for automotive applications, due to their low-temperature operation, low emissions and high efficiency. However, commercialization has been delayed for low durability, insufficient power density and expensive cost of platinum electrode [1]. Understanding on water and heat balance in a PEMFC should be on a higher plane to enhance both power density and durability, which will eventually decrease the cost per power required.

In the field of fuel cell engineering, water and heat management have been two major issues in designing a membrane electrode assembly (MEA) with excellent performance. During the last decade, a numbers of investigations have been reported on optimal design of MEA under consideration of agglomerated platinum electrode to analyze and mitigate drawbacks caused from imbalance of water and heat by means of computational fluid dynamics (CFD) modeling [2–9]. Among them, most of the investigations into PEMFC modeling [2–7] have focused on isothermal conditions due to the low variation of local temperature through the MEA, with exception of Shah et al. [8] and Gerteisen et al. [9]. They have implemented an agglomerate, non-isothermal model to enhance water management in a PEMFC, however, their interests were limited to the cathode of the MEA. It is critical to consider non-isothermal operation because the local distribution of cell temperature governs species diffusion, kinetics of electrochemical reactions and proton conductivity through Nafion. In addition, estimation of the amount of heat generation and temperature distribution through the MEA are crucial when condensation of water is dominant in cathode, even for a single cell with small MEA area [10].

In this paper, a non-isothermal and two-dimensional (2-D) agglomerate model is introduced to investigate heat balance through the MEA. Simulated polarization data of the base design were validated with experimental data from a previous study. In addition, an investigation of the relation between Nafion thickness and temperature distribution inside the MEA was undertaken.

## 2. Model formulation

### 2.1. Description of the PEMFC model

A cross-sectional 2-D MEA model was used for computational analysis. A five-layered MEA including an anode gas diffusion layer (AGDL), an anode catalyst layer (ACL), a proton exchange membrane (PEM), a cathode catalyst layer (CCL) and a cathode gas diffusion layer (CGDL) is illustrated in Fig. 1. Additionally, bold dark-blue dot line is drawn through the layer to calculate all through-plane data to characterized heat distributions in the MEA.

* Corresponding author. Tel.: +82 2 2220 0481; fax: +82 2 2298 5147.
*E-mail address:* scyi@hanyang.ac.kr (S.-C. Yi).

0306-2619/$ - see front matter © 2011 Elsevier Ltd. All rights reserved.
doi:10.1016/j.apenergy.2011.08.035

**Nomenclature**

| | |
|---|---|
| $a$ | roughness factor ($m^{-1}$) |
| ACL | anode catalyst layer |
| AGDL | anode gas diffusion layer |
| BP | bipolar plate |
| $C$ | molar concentration (mol $m^{-3}$) |
| CCL | cathode catalyst layer |
| CFD | computational fluid dynamics |
| CGDL | cathode gas diffusion layer |
| CL | catalyst layer |
| $c_p$ | heat capacity (J $kg^{-1}$ $K^{-1}$) |
| $D$ | diffusion coefficient ($m^2$ $s^{-1}$) |
| EOD | electro-osmotic drag |
| $E_r$ | effectiveness factor |
| EW | equivalent weight of Nafion (kg $mol^{-1}$) |
| $F$ | Faraday constant (C $mol^{-1}$) |
| GDL | gas diffusion layer |
| GFC | gas flow channel |
| $H$ | Henry's constant (mol (Pa $m^3$)$^{-1}$) |
| HOR | hydrogen oxidation reaction |
| $\vec{I}$ | current density vector (A $m^{-2}$) |
| $i$ | averaged current density (A $m^{-2}$) |
| $j_0$ | exchange current density (A $m^{-2}$) |
| $K$ | permeability ($m^2$) |
| $K$ | Nafion adsorption/desorption constant ($s^{-1}$) |
| $k_c$ | reaction rate constant ($s^{-1}$) |
| $k_{con}$ | condensation rate constant ($s^{-1}$) |
| $k_{eva}$ | evaporation rate constant ((atm s)$^{-1}$) |
| $k_{\text{th}}$ | thermal conductivity (W $m^{-1}$ $K^{-1}$) |
| $L$ | thickness (m) |
| $M$ | molecular weight (kg $mol^{-1}$) |
| MEA | membrane electrode assembly |
| $n_d$ | electro-osmotic drag coefficient |
| ORR | oxygen reduction reaction |
| $P$ | pressure (Pa) |
| $p_c$ | capillary pressure (Pa) |
| PEM | proton exchange membrane |
| PEMFC | proton exchange membrane fuel cell |
| $R$ | gas constant (J (mol K)$^{-1}$) |
| $r$ | radius (m) |
| $S$ | source/sink rate |
| $s$ | saturation |
| $T$ | cell temperature (K) |
| **u** | velocity (m $s^{-1}$) |
| UDF | user defined function |
| **W** | width (m) |
| $x$ | molar fraction |

*Greek letters*

| | |
|---|---|
| $\delta$ | thickness of electrolyte covering catalyst particles (m) |
| $\varepsilon$ | volume fraction |
| $\eta$ | overpotential |
| $\theta_c$ | contact angle (°) |
| $\kappa$ | electronic conductivity (S $m^{-1}$) |
| $\lambda$ | water content |
| $\mu$ | viscosity (kg $m^{-1}$ $s^{-1}$) |
| $\rho$ | density (kg $m^{-3}$) |
| $\sigma$ | surface tension (N $m^{-1}$) |
| $\Phi$ | phase potential (V) |
| $\Omega_T$ | convective heat transfer coefficient (J $K^{-1}$ $m^{-2}$ $s^{-1}$) |

*Superscripts*

| | |
|---|---|
| 0 | reference quantity |
| *eff* | effective quantity |
| *sat* | saturated quantity |

*Subscripts*

| | |
|---|---|
| *a* | anode |
| *abs* | absolute quantity |
| *agg* | agglomerate |
| *c* | cathode |
| *ch* | channel |
| CL | catalyst layer |
| *dry* | dry state |
| *e* | electrolyte phase |
| *Eq* | equilibrium |
| *g* | gas |
| GDL | gas diffusion layer |
| *H* | Heyrovsky–Volmer |
| $H_2$ | hydrogen |
| $H_2O$ | water |
| *l* | liquid |
| *m* | mass |
| *mem* | membrane |
| N112 | Nafion 112 |
| N115 | Nafion 115 |
| N117 | Nafion 117 |
| $O_2$ | oxygen |
| *pc* | phase change |
| *rg* | relative quantity of gas-phase |
| *rl* | relative quantity of liquid-phase |
| *s* | solid phase |
| *sat* | saturation |
| *T* | cell temperature |
| *T* | Tafel–Volmer |
| *v* | void phase |
| *w* | water |

In this study, catalyst layer (CL) modeling was performed based on the formation of the flooded agglomerates. Since Springer and Raistrick [11] presented the flooded agglomerate that includes Pt/C catalyst, Nafion ionomer, and macro- and micro-pores, it has recently dragged attractions to perform realistic simulation inside the CL. The major assumptions made to formulate the model are listed below:

- Steady-state and non-isothermal operation.
- Agglomerated structure formation inside the CL.
- The transport of the three phases of water in a PEMFC was considered.
- Solid- and electrolyte-phase potentials were used to describe electron and proton transport, respectively.
- Dual-pathway kinetics and Tafel kinetics were considered for the hydrogen oxidation reaction (HOR) and the oxygen reduction reaction (ORR), respectively.

### 2.2. Thermal model

Typically, a general energy-conservative equation can be expressed as:

$$\nabla \cdot (\rho c_p \mathbf{u}_g T) = \nabla \cdot (k_{th} \nabla T) + S_T \quad (1)$$

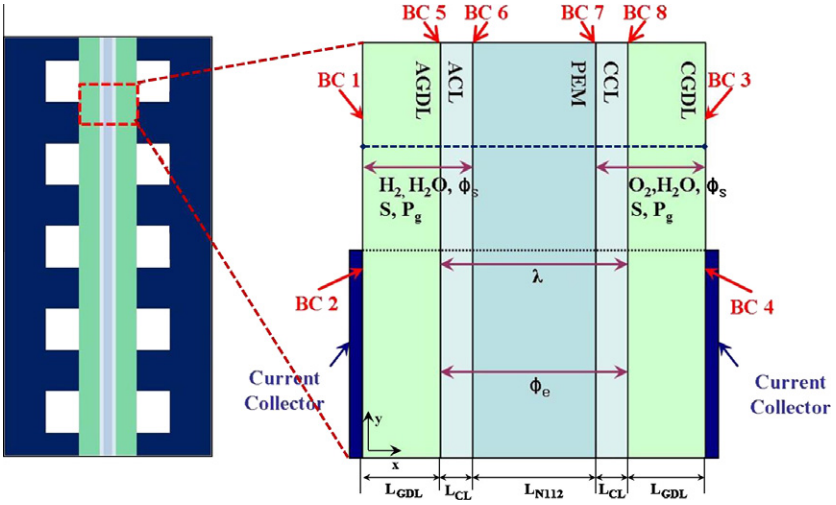


**Fig. 1.** A schematic of the cross-section of the MEA in a PEMFC.

**Table 1**
Governing equations in the present model [16,21].

| Layer | Governing equations | Eq. |
|---|---|---|
| AGDL | $0 = \nabla \cdot \left(\frac{K_{abs}K_{rg}}{\mu_{g,a}} \nabla P_g\right)$ | (12) |
| | $\nabla \cdot (\mathbf{u}_g C_{H_2,g}) = \nabla \cdot \left(\varepsilon_{v,\mathrm{GDL}}^{1.5}(1-s)^{1.5} D_{H_2,a}^0 \left(\frac{T}{T^0}\right)^{1.5} \left(\frac{P^0}{P}\right) \nabla C_{H_2,g}\right) + S_{H_2,g}$ | (13) |
| | $\nabla \cdot (\mathbf{u}_g C_{H_2O,g}) = \nabla \cdot \left(\varepsilon_{v,\mathrm{GDL}}^{1.5}(1-s)^{1.5} D_{H_2O,a}^0 \left(\frac{T}{T^0}\right)^{1.5} \left(\frac{P^0}{P}\right) \nabla C_{H_2O,g}\right) + S_{H_2O,g}$ | (14) |
| | $0 = \nabla \cdot \left(\left(-\frac{\rho_l K_{abs} K_{rl}}{\mu_l} \cdot \frac{dp_c}{ds}\right) \nabla s\right) + S_{sat}$ | (15) |
| | $0 = \nabla \cdot \left(\varepsilon_{s,\mathrm{GDL}}^{1.5} \kappa_s \nabla \Phi_s\right)$ | (16) |
| | $\nabla \cdot (\rho c_p \mathbf{u}_g T) = \nabla \cdot (k_{\mathrm{th,GDL}} \nabla T) + S_T$ | (17) |
| CGDL | $0 = \nabla \cdot \left(\frac{K_{abs}K_{rg}}{\mu_{g,c}} \nabla P_g\right)$ | (18) |
| | $\nabla \cdot (\mathbf{u}_g C_{O_2,g}) = \nabla \cdot \left(\varepsilon_{v,\mathrm{GDL}}^{1.5}(1-s)^{1.5} D_{O_2,c}^0 \left(\frac{T}{T^0}\right)^{1.5} \left(\frac{P^0}{P}\right) \nabla C_{O_2,g}\right) + S_{O_2,g}$ | (19) |
| | $\nabla \cdot (\mathbf{u}_g C_{H_2O,g}) = \nabla \cdot \left(\varepsilon_{v,\mathrm{GDL}}^{1.5}(1-s)^{1.5} D_{H_2O,c}^0 \left(\frac{T}{T^0}\right)^{1.5} \left(\frac{P^0}{P}\right) \nabla C_{H_2O,g}\right) + S_{H_2O,g}$ | (20) |
| | $0 = \nabla \cdot \left(\left(-\frac{\rho_l K_{abs} K_{rl}}{\mu_l} \cdot \frac{dp_c}{ds}\right) \nabla s\right) + S_{sat}$ | (21) |
| | $0 = \nabla \cdot \left(\varepsilon_{s,\mathrm{GDL}}^{1.5} \kappa_s \nabla \Phi_s\right)$ | (22) |
| | $\nabla \cdot (\rho c_p \mathbf{u}_g T) = \nabla \cdot (k_{\mathrm{th,GDL}} \nabla T) + S_T$ | (23) |
| ACL | $0 = \nabla \cdot \left(\frac{K_{abs}K_{rg}}{\mu_{g,a}} \nabla P_g\right) + S_m$ | (24) |
| | $\nabla \cdot (\mathbf{u}_g C_{H_2,g}) = \nabla \cdot \left(\varepsilon_{v,\mathrm{CL}}^{1.5}(1-s)^{1.5} D_{H_2,a}^0 \left(\frac{T}{T^0}\right)^{1.5} \left(\frac{P^0}{P}\right) \nabla C_{H_2,g}\right) + S_{H_2,g}$ | (25) |
| | $\nabla \cdot (\mathbf{u}_g C_{H_2O,g}) = \nabla \cdot \left(\varepsilon_{v,\mathrm{CL}}^{1.5}(1-s)^{1.5} D_{H_2O,a}^0 \left(\frac{T}{T^0}\right)^{1.5} \left(\frac{P^0}{P}\right) \nabla C_{H_2O,g}\right) + S_{H_2O,g}$ | (26) |
| | $0 = \nabla \cdot (\varepsilon_{\mathrm{CL}}^{1.5} D_\lambda \nabla \lambda) + S_\lambda$ | (27) |
| | $0 = \nabla \cdot \left(\left(-\frac{\rho_l K_{abs} K_{rl}}{\mu_l} \cdot \frac{dp_c}{ds}\right) \nabla s\right) + S_{sat}$ | (28) |
| | $0 = \nabla \cdot \left(\varepsilon_{e,\mathrm{CL}}^{1.5} \kappa_e \nabla \Phi_e\right) + S_{\Phi_e}$ | (29) |
| | $0 = \nabla \cdot \left(\varepsilon_{s,\mathrm{CL}}^{1.5} \kappa_s \nabla \Phi_s\right) + S_{\Phi_s}$ | (30) |
| | $\nabla \cdot (\rho c_p \mathbf{u}_g T) = \nabla \cdot (k_{\mathrm{th,CL}} \nabla T) + S_T$ | (31) |
| CCL | $0 = \nabla \cdot \left(\frac{K_{abs}K_{rg}}{\mu_{g,c}} \nabla P_g\right) + S_m$ | (32) |
| | $\nabla \cdot (\mathbf{u}_g C_{O_2,g}) = \nabla \cdot \left(\varepsilon_{v,\mathrm{CL}}^{1.5}(1-s)^{1.5} D_{O_2,c}^0 \left(\frac{T}{T^0}\right)^{1.5} \left(\frac{P^0}{P}\right) \nabla C_{O_2,g}\right) + S_{O_2,g}$ | (33) |
| | $\nabla \cdot (\mathbf{u}_g C_{H_2O,g}) = \nabla \cdot \left(\varepsilon_{v,\mathrm{CL}}^{1.5}(1-s)^{1.5} D_{H_2O,c}^0 \left(\frac{T}{T^0}\right)^{1.5} \left(\frac{P^0}{P}\right) \nabla C_{H_2O,g}\right) + S_{H_2O,g}$ | (34) |
| | $0 = \nabla \cdot \left(\varepsilon_{e,\mathrm{CL}}^{1.5} D_\lambda \nabla \lambda\right) + S_\lambda$ | (35) |
| | $0 = \nabla \cdot \left(\left(-\frac{\rho_l K_{abs} K_{rl}}{\mu_l} \cdot \frac{dp_c}{ds}\right) \nabla s\right) + S_{sat}$ | (36) |
| | $0 = \nabla \cdot \left(\varepsilon_{e,\mathrm{CL}}^{1.5} \kappa_e \nabla \Phi_e\right) + S_{\Phi_e}$ | (37) |
| | $0 = \nabla \cdot \left(\varepsilon_{s,\mathrm{CL}}^{1.5} \kappa_s \nabla \Phi_s\right) + S_{\Phi_s}$ | (38) |
| | $\nabla \cdot (\rho c_p \mathbf{u}_g T) = \nabla \cdot (k_{\mathrm{th,CL}} \nabla T) + S_T$ | (39) |
| PEM | $0 = \nabla \cdot \left(\frac{\rho_{mem,dry}}{\mathrm{EW}} D_\lambda \nabla \lambda\right) + S_\lambda$ | (40) |
| | $0 = \nabla \cdot (\kappa_e \nabla \Phi_e)$ | (41) |
| | $0 = \nabla \cdot (k_{\mathrm{th},mem} \nabla T) + S_T$ | (42) |

where $\rho c_p$ and $k_{\text{th}}$ are heat capacitance and thermal conductivity of the mixture, respectively. The heat capacitance of the mixture, $\rho c_p$, is defined as:

$$\rho c_p = s(\rho c_p)_l + (1-s)(\rho c_p)_g \tag{2}$$

where $(\rho c_p)_g$ and $(\rho c_p)_l$ are heat capacitance of gas mixture and liquid water, respectively. The gas-phase velocity, $\mathbf{u}_g$, is calculated by Darcy's law, disregarding the gravity term

$$\mathbf{u}_g = -\frac{K_{abs}K_{rg}}{\mu_g}\nabla P_g \tag{3}$$

where $K_{abs}$ is absolute permeability, and $k_{rg}$, $\mu_g$, and $P_g$ are relative permeability, viscosity, and pressure of gas-phase, respectively.

The heat generation/depletion term, $S_T$, includes four different physical effects arising from different sources, that is thermodynamic irreversibility, heat generation by exothermic reaction, electron and proton transport resistance and the phase change of water. Due to complexity of the CL, all four sources of heat generation are combined to explain heat transfer in PEMFC.

For thermal boundary condition, two different types of boundary conditions are used for gas diffusion layer (GDL)/gas flow channel (GFC) and GDL/bipolar plate (BP) interfaces. In general fuel cell operation, the bipolar plate is maintained at fixed temperature, while excessive heat generated during the operation is removed by convection of the flow in channel. Therefore, the boundary conditions at GDL/GFC and GDL/BP interfaces are as:

$$\begin{cases} \frac{\partial T}{\partial n} = -\Omega_T(T - T_{\text{GFC}}) & (\text{at BC1 and BC3}) \\ T = T_{\text{GFC}} & (\text{at BC2 and BC4}) \end{cases} \tag{4}$$

All of the governing equations and the source terms of the nine dependent variables considered in the proposed model – namely, molar concentration of hydrogen, oxygen and water vapor,

**Table 2**
Source terms in the present model [5,6].

| Layer | Variables | Source Term | Eq. |
|---|---|---|---|
| ACL | $H_2$ | $S_{H_2,g} = \underbrace{-\frac{P_{H_2}}{H_{H_2,e}}\left(\frac{1}{E_r k_{c,a}(1-\varepsilon_{v,\text{CL}})} + \frac{(r_{agg}+\delta_{agg})\delta_{agg}}{a_{agg}r_{agg}D_{H_2,e}} + \frac{(r_{agg}+\delta_{agg}+\delta_w)\delta_w H_{H_2,w}}{a_{agg}(r_{agg}+\delta_{agg})D_{H_2,w}H_{H_2,e}}\right)^{-1}}_{\text{depletion by HOR in ACL}}$ | (43) |
| | $H_2O$ | $S_{H_2O,g} = \underbrace{-k\frac{\rho_{dry,mem}}{\text{EW}}(\lambda_{eq}-\lambda)}_{\text{depletion by water uptake}} \quad \underbrace{-\frac{S_{pc}}{M_{H_2O}}}_{\substack{\text{gas-phase water generation/} \\ \text{depletion by phase change}}}$ | (44) |
| | $\lambda$ | $S_\lambda = \underbrace{k\frac{\rho_{mem,dry}}{\text{EW}}(\lambda_{eq}-\lambda)}_{\text{generation by water uptake}} \quad \underbrace{-\nabla\cdot\left(\frac{n_d}{F}\vec{I}\right)}_{\substack{\text{depletion by} \\ \text{electro-osmotic drag(EOD)}}}$ | (45) |
| | $S$ | $S_{sat} = \underbrace{\nabla\cdot\left[\left(\frac{\rho_l K_{abs}K_{rl}}{\mu_l}\right)\nabla P_g\right]}_{\substack{\text{induced transport due to} \\ \text{gas-phase pressure gradient}}} + \underbrace{S_{pc}}_{\substack{\text{liquid-phase water generation/} \\ \text{depletion by phase change}}}$ | (46) |
| | $\Phi_e$ | $S_{\Phi_e} = \underbrace{2F\frac{P_{H_2}}{H_{H_2,e}}\left(\frac{1}{E_r k_{c,a}(1-\varepsilon_{v,\text{CL}})} + \frac{(r_{agg}+\delta_{agg})\delta_{agg}}{a_{agg}r_{agg}D_{H_2,e}} + \frac{(r_{agg}+\delta_{agg}+\delta_w)\delta_w H_{H_2,w}}{a_{agg}(r_{agg}+\delta_{agg})D_{H_2,w}H_{H_2,e}}\right)^{-1}}_{\text{ionic charge generation by HOR}}$ | (47) |
| | $\Phi_s$ | $S_{\Phi_s} = \underbrace{-2F\frac{P_{H_2}}{H_{H_2,e}}\left(\frac{1}{E_r k_{c,a}(1-\varepsilon_{v,\text{CL}})} + \frac{(r_{agg}+\delta_{agg})\delta_{agg}}{a_{agg}r_{agg}D_{H_2,e}} + \frac{(r_{agg}+\delta_{agg}+\delta_w)\delta_w H_{H_2,w}}{a_{agg}(r_{agg}+\delta_{agg})D_{H_2,w}H_{H_2,e}}\right)^{-1}}_{\text{electric charge depletion by HOR}}$ | (48) |
| | $T$ | $S_T = \underbrace{\frac{S_{\Phi_e}}{2F}\times T\Delta S}_{\text{reversible heat of rxn}} + \underbrace{S_{\Phi_e}\times\eta_a}_{\text{irreversible heat of rxn}} + \underbrace{\frac{i_e^2}{\kappa_e^{eff}} + \frac{i_s^2}{\kappa_s^{eff}}}_{\text{Ohmic heating}} + \underbrace{h_{pc}S_{pc}}_{\substack{\text{heat release/absorption due to} \\ \text{water condensation/evaporation}}}$ | (49) |
| PEM | $\lambda$ | $S_\lambda = \underbrace{-\nabla\cdot\left(\frac{n_d}{F}\vec{I}\right)}_{\text{depletion by EOD}}$ | (50) |
| | $T$ | $S_T = i_e^2/\kappa_e^{eff}$ | (51) |
| CCL | $O_2$ | $S_{O_2} = \underbrace{-\frac{P_{O_2}}{H_{O_2,e}}\left(\frac{1}{E_r k_{c,c}(1-\varepsilon_{v,\text{CL}})} + \frac{(r_{agg}+\delta_{agg})\delta_{agg}}{a_{agg}r_{agg}D_{O_2,e}} + \frac{(r_{agg}+\delta_{agg}+\delta_w)\delta_w H_{O_2,w}}{a_{agg}(r_{agg}+\delta_{agg})D_{O_2,w}H_{O_2,e}}\right)^{-1}}_{\text{depletion by ORR}}$ | (52) |
| | $H_2O$ | $S_{H_2O,g} = \underbrace{-k\frac{\rho_{dry,mem}}{\text{EW}}(\lambda_{eq}-\lambda)}_{\text{depletion by water uptake}} + \underbrace{\frac{2P_{O_2}}{H_{O_2,e}}\left(\frac{1}{E_r k_{c,c}(1-\varepsilon_{v,\text{CCL}})} + \frac{(r_{agg}+\delta_{agg})\delta_{agg}}{a_{agg}r_{agg}D_{O_2,e}} + \frac{(r_{agg}+\delta_{agg}+\delta_w)\delta_w H_{O_2,w}}{a_{agg}(r_{agg}+\delta_{agg})D_{O_2,w}H_{O_2,e}}\right)^{-1}}_{\text{generation by ORR}} \quad \underbrace{-\frac{S_{pc}}{M_{H_2O}}}_{\substack{\text{gas-phase water generation/} \\ \text{depletion by phase change}}}$ | (53) |
| | $\lambda$ | $S_\lambda = \underbrace{k\frac{\rho_{dry,mem}}{\text{EW}}(\lambda_{eq}-\lambda)}_{\text{generation by water uptake}} \quad \underbrace{-\nabla\cdot\left(\frac{n_d}{F}\vec{I}\right)}_{\text{generation by EOD}}$ | (54) |
| | $S$ | $S_{sat} = \underbrace{\nabla\cdot\left[\left(\frac{\rho_l K_{abs}K_{rl}}{\mu_l}\right)\nabla P_g\right]}_{\substack{\text{induced transport due to} \\ \text{gas-phase pressure gradient}}} + \underbrace{S_{pc}}_{\substack{\text{liquid-phase water generation/} \\ \text{depletion by phase change}}}$ | (55) |
| | $\Phi_e$ | $S_{\Phi_e} = \underbrace{-4F\frac{P_{O_2}}{H_{O_2,e}}\left(\frac{1}{E_r k_{c,c}(1-\varepsilon_{v,\text{CL}})} + \frac{(r_{agg}+\delta_{agg})\delta_{agg}}{a_{agg}r_{agg}D_{O_2,e}} + \frac{(r_{agg}+\delta_{agg}+\delta_w)\delta_w H_{O_2,w}}{a_{agg}(r_{agg}+\delta_{agg})D_{O_2,w}H_{O_2,e}}\right)^{-1}}_{\text{ionic charge depletion by ORR}}$ | (56) |
| | $\Phi_s$ | $S_{\Phi_s} = \underbrace{4F\frac{P_{O_2}}{H_{O_2,e}}\left(\frac{1}{E_r k_{c,c}(1-\varepsilon_{v,\text{CL}})} + \frac{(r_{agg}+\delta_{agg})\delta_{agg}}{a_{agg}r_{agg}D_{O_2,e}} + \frac{(r_{agg}+\delta_{agg}+\delta_w)\delta_w H_{O_2,w}}{a_{agg}(r_{agg}+\delta_{agg})D_{O_2,w}H_{O_2,e}}\right)^{-1}}_{\text{electric charge generation by ORR}}$ | (57) |
| | $T$ | $S_T = \underbrace{-\frac{S_{\Phi_e}}{4F}\times T\Delta S}_{\text{reversible heat of rxn}} + \underbrace{-S_{\Phi_e}\times\eta_c}_{\text{irreversible heat of rxn}} + \underbrace{\frac{i_e^2}{\kappa_e^{eff}} + \frac{i_s^2}{\kappa_s^{eff}}}_{\text{Ohmic heating}} + \underbrace{h_{pc}S_{pc}}_{\substack{\text{heat release/absorption due to} \\ \text{water condensation/evaporation}}}$ | (58) |

electrolyte-phase water content, liquid water saturation, solid-phase potential, electrolyte-phase potential, gas-phase pressure, and cell temperature, – are listed in Table 1. Also, the corresponding source terms are listed in Table 2.

The liquid water transport in the GDL and CL can be influenced by the capillary pressure. Eq. (5) defines the capillary pressure as a function of Leverette term [12]:

$$p_c = \sigma\left(\frac{\varepsilon_v}{K_{abs}}\right)^{0.5}\cos(\theta_c)J(s) \tag{5}$$

In addition, the source/sink term for the generation/depletion of liquid water due to phase change, $S_{pc}$, is defined as:

$$S_{pc} = \begin{cases} k_{con}\varepsilon_v x_{H_2O}\left(C_{H_2O} - \frac{P^{sat}_{H_2O}}{RT}\right)M_{H_2O} & \text{if } C_{H_2O} > C^{sat}_{H_2O} \\ -k_{eva}\varepsilon_v s\rho_l\left(\frac{P^{sat}_{H_2O}}{RT} - C_{H_2O}\right) & \text{if } C_{H_2O} < C^{sat}_{H_2O} \end{cases} \tag{6}$$

where $k_{con}$ and $k_{eva}$ are the condensation and evaporation rate constants, respectively.

### 2.3. Electrochemical Model

As already mentioned in the section 2.1, the kinetics of the HOR and ORR are dominated by a combination of Tafel–Volmer and Heyrovsky–Volmer reactions [13] and Tafel reaction [5] in ACL and CCL. The reaction rate constant for ACL and CCL can be defined as:

$$k_{c,a} = \frac{A_v}{2F(1-\varepsilon_{v,cl})c^0_{H_2}}\left\{\begin{array}{c} j_{0,T}\left[1 - exp\left(-\frac{2F\eta_a}{\gamma RT}\right)\right] + j_{0,H}\left[exp\left(-\frac{2F\eta_a}{\gamma RT}\right)\right. \\ \left. -exp\left(-\frac{F\eta_a}{\gamma RT}\right)\times exp\left(-\frac{F\eta_a}{2RT}\right)\right] \end{array}\right\} \tag{7}$$

$$k_{c,c} = \frac{A_v j_{0,c}}{4F(1-\varepsilon_{v,cl})c^0_{O_2}}exp\left(-\frac{2F\eta_c}{RT}\right) \tag{8}$$

where $j_{0,T} = 0.47$ A cm$^{-2}$, $j_{0,H} = 0.01$ A cm$^{-2}$ and $\gamma = 1.2$. The overpotential of the electrode, $\eta$, is defined as follows:

$$\eta = \Phi_s - \Phi_e \tag{9}$$

The effectiveness factor is given by the following equation:

$$E_r = \frac{1}{\phi_L}\left(\frac{1}{\tanh(3\phi_L)} - \frac{1}{3\phi_L}\right) \tag{10}$$

And the Thiele's modulus for the spherical agglomerate is defined by

$$\phi_L = \frac{r_{agg}}{3}\sqrt{\frac{k_c}{D_e}} \tag{11}$$

where $r_{agg}$ and $D_e$ are the radius of agglomerate and diffusion coefficient of $H_2$ and $O_2$ in Nafion, respectively.

### 2.4. Computational method

Nine governing equations and boundary conditions for each variable were used to numerically simulate the presented model using FLUENT, a CFD software package based on the finite volume method [14]. Because FLUENT does not contain an electrochemical modeling module and the source terms in the model are highly non-linear, all governing equations were modeled using user defined functions (UDFs) [15]. To mitigate the non-linearity due to the severe coupling and to increase the rate of convergence, the energy balance equation was involved after obtaining an isothermal solution. Two hours of average calculations on an Intel E8400 CPU were needed for each case to converge with all residuals under $10^{-9}$.

## 3. Results and discussions

### 3.1. Model validation

To evaluate the validity of the present model, a simulated polarization curve of the base design was compared with experimental data taken from Jung et al. [16]. The base design was operated by supplying fully saturated feed gas into the cell fixture at inlet temperature of 70 °C and ambient outlet pressure condition. Red solid/rectangular scatter line and blue dotted/circular scatter line in Fig. 2 represent the simulated/experimental cell polarization and the simulated/estimated heat release versus cell voltage, respectively. The comparisons of the results show that agreement

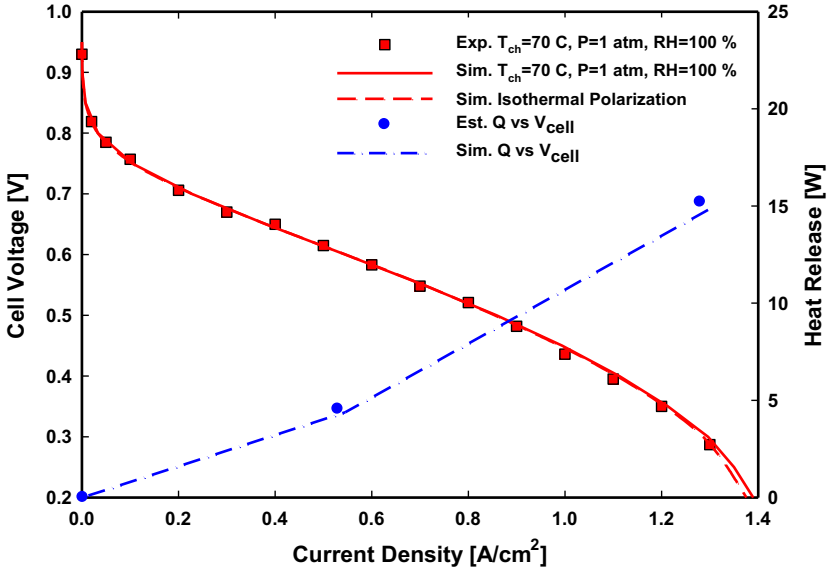


**Fig. 2.** Validation of the simulation data with experimental data [16].

**Table 3**
Transport and electrochemical parameters used in the model [5,13,16–19,21–26].

| Description | Value | Unit | Ref. |
|---|---|---|---|
| Thermal conductivity of CL, $k_{th,CL}$ | 2 | W m$^{-1}$ K$^{-1}$ | [17] |
| Thermal conductivity of Nafion, $k_{th,mem}$ | 0.30 | W m$^{-1}$ K$^{-1}$ | [18] |
| Diffusion coefficient of $H_2$ in anode (at 353 K, 1 atm), $D^0_{H_2,a}$ | $1.1028 \times 10^{-4}$ | m$^2$ s$^{-1}$ | [21] |
| Diffusion coefficient of $O_2$ in cathode (at 353 K, 1 atm), $D^0_{O_2,c}$ | $3.2348 \times 10^{-5}$ | m$^2$ s$^{-1}$ | [21] |
| Diffusion coefficient of $H_2O$ in anode (at 353 K, 1 atm), $D^0_{H_2O,a}$ | $1.1028 \times 10^{-4}$ | m$^2$ s$^{-1}$ | [21] |
| Diffusion coefficient of $H_2O$ in cathode (at 353 K, 1 atm), $D^0_{H_2O,c}$ | $3.8900 \times 10^{-5}$ | m$^2$ s$^{-1}$ | [21] |
| Diffusion coefficient of $H_2$ in Nafion, $D_{H_2,e}$ | $1.28 \times 10^{-9}$ | m$^2$ s$^{-1}$ | [22] |
| Diffusion coefficient of $O_2$ in Nafion, $D_{O_2,e}$ | $8.45 \times 10^{-10}$ | m$^2$ s$^{-1}$ | [23] |
| Henry constant for dissolution of $H_2$ in Nafion, $H_{H_2,e}$ | 66,900 | Pa m$^3$ mol$^{-1}$ | [22] |
| Henry constant for dissolution of $O_2$ in Nafion, $H_{O_2,e}$ | 31,664 | Pa m$^3$ mol$^{-1}$ | [23] |
| Cathode exchange current density, $j_{0,c}$ | $6.8 \times 10^{-5}$ | A m$^{-2}$ | [16] |
| Exchange current density of Tafel–Volmer kinetic, $j_{0,T}$ | 4700 | A m$^{-2}$ | [13] |
| Exchange current density of Heyrovsky–Volmer kinetic, $j_{0,H}$ | 100 | A m$^{-2}$ | [13] |
| Surface tension, $\sigma$ | 0.0625 | N m$^{-1}$ | [19] |
| Equivalent weight, EW | 1.1 | kg mol$^{-1}$ | [5] |
| Dry membrane density, $\rho_{mem,dry}$ | 2000 | kg m$^{-3}$ | [5] |
| Nafion adsorption/desorption constant, $k$ | 10,000 | s$^{-1}$ | [5] |
| Thickness of gas diffusion layer, $L_{GDL}$ | 0.00027 | m | [16] |
| Thickness of catalyst layer, $L_{CL}$ | 0.000055 | m | [16] |
| Thickness of Nafion 112, $L_{N112}$ | 0.000051 | m | [16] |
| Thickness of Nafion 115, $L_{N115}$ | 0.000128 | m | [20] |
| Thickness of Nafion 117, $L_{N117}$ | 0.000179 | m | [20] |
| Radius of an agglomerate, $r_{agg}$ | $1.0 \times 10^{-6}$ | m | [5] |
| Thickness of Nafion binder, $\delta_{agg}$ | $8.0 \times 10^{-8}$ | m | [5] |
| Heat capacitance of gas mixture, $(\rho c_p)_g$ | $4.187 \times 10^6$ | J m$^{-3}$ K$^{-1}$ | [24] |
| Heat capacitance of liquid water, $(\rho c_p)_l$ | $1.0 \times 10^3$ | J m$^{-3}$ K$^{-1}$ | [24] |
| Absolute permeability, $K_{abs}$ | $1.0 \times 10^{-12}$ | m$^2$ | Est. |
| Relative permeability of gas-phase, $K_{rg}$ | $(1-s)^3$ | | [24] |
| Relative permeability of liquid-phase, $K_{rl}$ | $s^3$ | | [24] |
| Liquid water density, $\rho_l$ | 998 | kg m$^{-3}$ | [21] |
| Liquid water viscosity, $\mu_l$ | $1.0 \times 10^{-3}$ | kg m$^{-1}$ s$^{-1}$ | [21] |
| Gas-phase viscosity in anode, $\mu_{g,a}$ | $8.4 \times 10^{-6}$ | kg m$^{-1}$ s$^{-1}$ | [21] |
| Gas-phase viscosity in cathode, $\mu_{g,c}$ | $1.8 \times 10^{-5}$ | kg m$^{-1}$ s$^{-1}$ | [21] |
| Reference temperature, $T^0$ | 353 | K | [21] |
| Reference pressure, $P^0$ | 101,325 | Pa | [21] |
| Volume fraction of void in GDL, $\varepsilon_{v,GDL}$ | 0.6 | – | [16] |
| Volume fraction of solid in GDL, $\varepsilon_{s,GDL}$ | 0.4 | – | [16] |
| Volume fraction of void in CL, $\varepsilon_{v,CL}$ | 0.639 | – | [16] |
| Volume fraction of solid in CL, $\varepsilon_{s,CL}$ | 0.186 | – | [16] |
| Volume fraction of electrolyte in CL, $\varepsilon_{e,CL}$ | 0.175 | – | [16] |
| Volume fraction of electrolyte inside the agglomerate, $\varepsilon_{agg}$ | 0.45 | – | [16] |
| Proton conductivity of Nafion, $\kappa_e$ $(0.5139\lambda - 0.326)\exp[1268(\frac{1}{303} - \frac{1}{T})]$ | | S m$^{-1}$ | [25] |
| Electron conductivity of carbon, $\kappa_s$ | 3264 | S m$^{-1}$ | [25] |
| Channel temperature, $T_{GFC}$ | 353 | K | [16] |
| Convective heat transfer coefficient, $\Omega_T$ | $1.0 \times 10^3$ | J K$^{-1}$ m$^{-2}$ s$^{-1}$ | Est. |
| Contact angle of CL, $\theta_{c,CL}$ | 110 | ° | [16] |
| Contact angle of GDL, $\theta_{c,GDL}$ | 130 | ° | [16] |
| Electro-osmotic drag coefficient, $n_d$ | $\frac{2.5\lambda}{22}$ | – | [25] |
| Heat of vaporization/condensation, $h_{pc}$ | $40.7 \times 10^3$ | J mol$^{-1}$ | [21] |
| Thickness of water layer covering an agglomerate, $\delta_w$ | $\frac{\varepsilon_{v,CL}s}{a_{agg}}$ | m | [26] |
| Agglomerate surface area per unit volume, $a_{agg}$ | $\frac{3\varepsilon_{s,CL}\varepsilon_{v,CL}}{r_{agg}(1-\varepsilon_{agg})}$ | m$^{-1}$ | [26] |

Est.: estimated.

between the numerical and experimental data was sufficient to confirm the validity of the simulated cell polarization. For cell temperature, however, thermal model is hard to be verified with the cell polarization, since the temperature difference is below 10 K, although the cell operates under high current density. Therefore, simulated heat release is compared with the estimated heat release from the experimental cell polarization when high heating value of the enthalpy-based voltage is assumed as 1.48 V. All transport variables and operating conditions including the structural designs used in this work are noted in Table 3.

Through this investigation, the authors were intended to relate various heat release modes and heat transfer to cell temperature distribution in MEA. Therefore, further investigations were performed on: (i) the temperature distribution throughout the MEA and (ii) the effect of Nafion thickness on cell temperature distribution.

### 3.2. Temperature distribution inside the MEA

Fig. 3 shows the temperature distribution in the MEA with increasing current. In Fig. 3a, cell temperature contours through all five layers are given at cell voltages of 0.70 V, 0.50 V and 0.30 V, which in this system are equivalent to low, intermediate and high current densities, respectively. As shown in the figure, the temperature difference between the anode and cathode is increased as the current density was increased, due to the electrochemical reaction. In the CCL, the cell temperature at 0.30 V was higher under the channel than that under the shoulder, approximately 349 K. This result was mainly due to the difference in the current density distribution because the reaction rate is enhanced in the area under the channel. This difference can be dominant, especially when mass transport limitation occurs. In addition, cell temperature distribution along the through-plane direction is

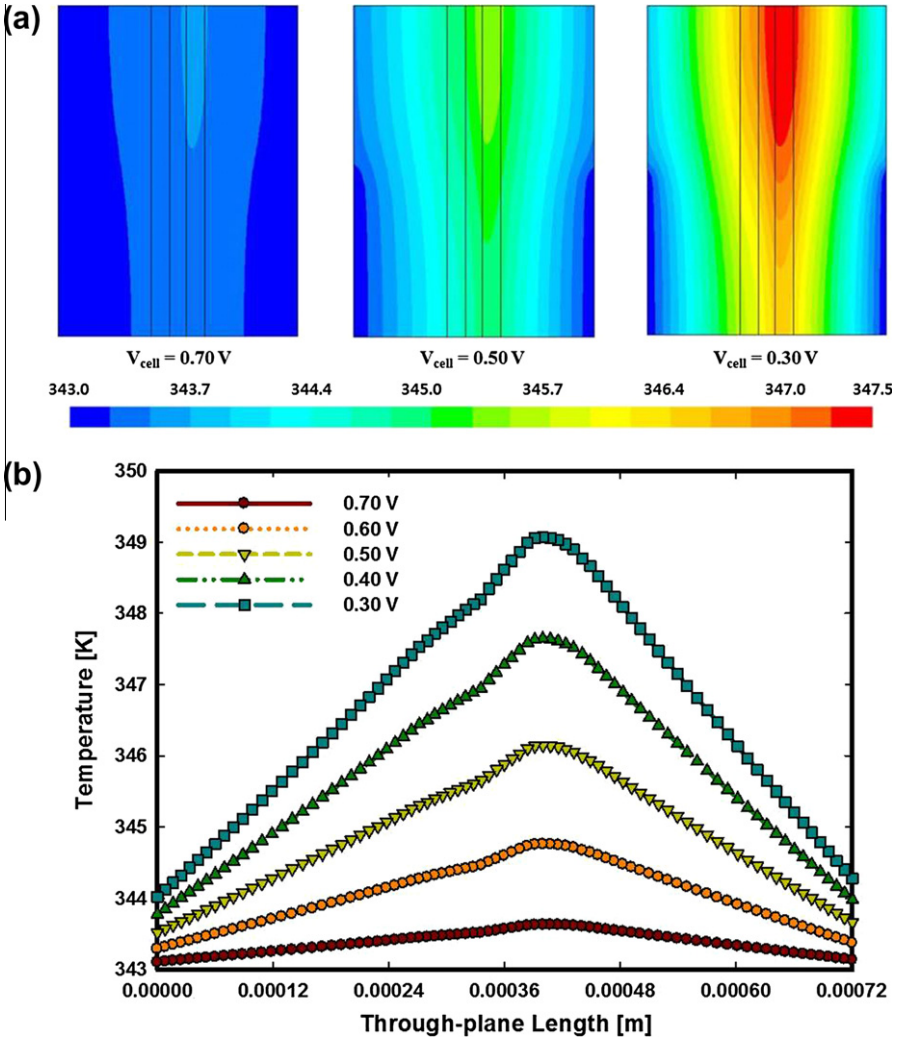


**Fig. 3.** Cell temperature distribution in the MEA – (a) temperature contours at 0.70 V, 0.50 V and 0.30 V and (b) temperature distribution in the through-plane direction at 0.70 V, 0.60 V, 0.50 V, 0.40 V and 0.30 V.

presented in Fig 3b. Here, the cell temperature increased as current density was increased, due to the increased heat generation by irreversible heat of reaction and charge transfer resistance. Because of the relatively low thermal conductivity of the PEM [17,18], the temperature gradient in through-plane direction was particularly high.

### 3.3. Effect of Nafion thickness

As Nafion thickness increases, the proton transfer resistance and diffusive resistance of water transfer through PEM are increased [19,20]. These results indicate that PEM is a separator that controls water and heat balance between the anode and the cathode, therefore cell temperature distribution can be significantly affected by Nafion thickness. Because the difference in cell performance varies the heat release in the MEA, the simulation was performed when total heat release is fixed as 10,000 W $m^{-2}$.

Fig. 4a shows the cell temperature distributions for Nafion 112, 115 and 117 MEAs when cell voltages are 0.46 V, 0.40 V and 0.366 V, respectively. Among them, Nafion 117 MEA was expected to have the highest cell temperature in the CCL. Because most of the heat releases by the ORR in the CCL, the increased thickness of Nafion can act as an additional heat transfer barrier, which disturbs heat transfer from CCL to anode side. This tendency can be seen clearly in the Fig. 4b. The cell temperature in the cathode is increased with increasing Nafion thickness, because of the heat accumulation. However, the cell temperature distributions were similar in the anode.

## 4. Conclusions

A non-isothermal PEMFC model based on agglomerated electrode formation was presented that takes into account various heat generation sources including reversible/irreversible heat release, ohmic heating and the phase change of water. Employing this model, the temperature distribution inside the MEA was predicted. In addition, the effect of Nafion thickness was investigated to clarify its influence on the cell temperature distribution. Despite a few limitations of the present model, the following conclusions can be drawn:

(i) The model was successfully validated by its agreement with the experimental data. In addition, the simulated total heat releases at different cell voltages were cross-checked to confirm reliability of the model. In this work, it was of key importance to properly model energy balance, because the local cell temperature distribution governs water balance in PEMFC.

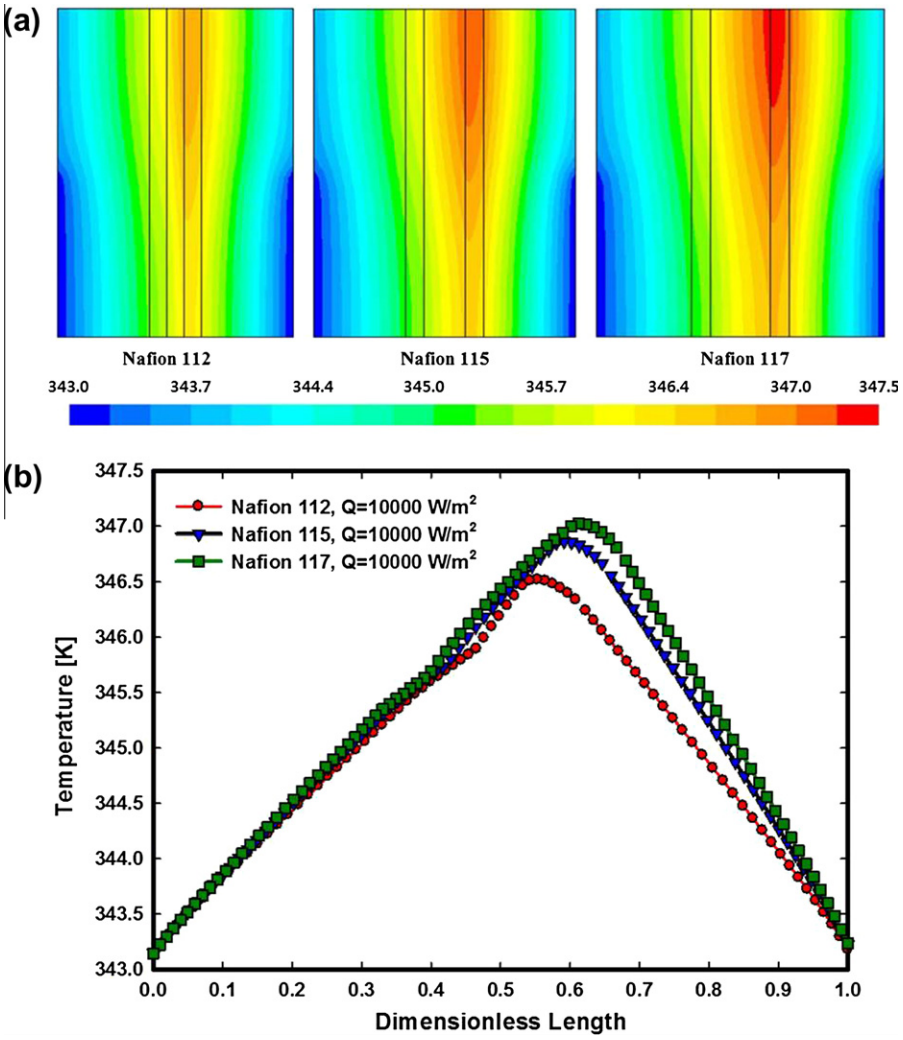


**Fig. 4.** Cell temperature distribution in the MEA with Nafion 112, 115 and 117 when total heat release is fixed at 10,000 W $m^{-2}$ – (a) cell temperature contours and (b) cell temperature distribution in the through-plane direction.

(ii) Effect of Nafion thickness on the cell temperature variation was investigated using the model. The cell temperature was increased in the cathode with increasing Nafion thickness, especially in the area under the channel. It can be deduced that the increased thermal resistance with increasing Nafion thickness resulted in more heat accumulation in the cathode, leading to cell temperature rise, due to relatively low thermal conductivity of Nafion.

## Acknowledgements

This work was supported by the Manpower Development Program for Energy & Resources funded by the Ministry of Knowledge and Economy, Republic of Korea. It was also partially supported by the Basic Science Research Program through the National Research Foundation of Korea funded by the Ministry of Education, Science and Technology (2010-0024794). The authors are grateful for their financial support.

## References

[1] Trongchuankij W, Pruksathorn K, Hunsom M. Preparation of a high performance Pt–Co/C electrocatalyst for oxygen reduction in PEM fuel cell via a combined process of impregnation and seeding. Appl Energy 2011;88:974–80.

[2] Secanell M, Carnes B, Suleman A, Djilali N. Numerical optimization of proton exchange membrane fuel cell cathodes. Electrochim Acta 2007;52:2668–82.

[3] Yin KM. A thin-film/agglomerate model of a proton-exchange-membrane fuel cell cathode catalyst layer with consideration of solid-polymer-electrolyte distribution. J Appl Electrochem 2007;37:971–82.

[4] Secanell M, Karan K, Suleman A, Djilali N. Multi-variable optimization of PEMFC cathodes using an agglomerate model. Electrochim Acta 2007;52:6318–37.

[5] Secanell M, Songprakorp R, Suleman A, Djilali N. Multi-objective optimization of a polymer electrolyte fuel cell membrane electrode assembly. Energy Environ Sci 2008;1:378–88.

[6] Jung CY, Kim WJ, Yi SC. Computational analysis of polarizations in membrane-electrode-assembly for proton exchange membrane fuel cells. J Membrane Sci 2009;341:5–10.

[7] Kamarajugadda S, Mazumder S. Numerical investigation of the effect of cathode catalyst layer structure and composition on polymer electrolyte membrane fuel cell performance. J Power Sources 2008;183:629–42.

[8] Shah AA, Kim GS, Gervais W, Young A, Promislow K, Li J, et al. The effect of water and microstructure on the performance of polymer electrolyte fuel cells. J Power Sources 2006;160:1251–68.

[9] Gerteisen D, Heilmann T, Ziegler C. Modeling the phenomena of dehydration and flooding of a polymer electrolyte membrane fuel cell. J Power Sources 2009;187:165–81.

[10] Siegel C. Review of computational heat and mass transfer modeling in polymer-electrolyte- membrane (PEM) fuel cells. Energy 2008;33:1331–52.

[11] Springer TE, Raistrick ID. Electrical impedance of a pore wall for the flooded-agglomerate model of porous gas diffusion electrodes. J Electrochem Soc 1989;136:1594–603.

[12] Leverette MC. Capillary behavior in porous solids. AIME Trans 1941;142:152–69.

[13] Wang JX, Springer TE, Azdic RR. Dual-pathway kinetic equation for the hydrogen oxidation reaction on Pt electrodes. J Electrochem Soc 2006;153:A1732–40.
[14] Patankar SV. Numerical heat transfer and fluid flow. Washington, DC: Hemisphere Publishing Corporation; 1980.
[15] Fluent 6.3 UDF Guide. New Hampshire: Fluent Inc.; 2005.
[16] Jung CY, Park CH, Lee YM, Kim WJ, Yi SC. Numerical analysis of catalyst agglomerates and liquid water transport in proton exchange membrane fuel cells. Int J Hydrogen Energy 2010;35:8433–45.
[17] Ju HC, Wang CY, Cleghorn S, Beuscher U. Nonisothermal modeling of polymer electrolyte fuel cells - I. Experimental validation. J Electrochem Soc 2005;152:A1645–53.
[18] Khandelwal M, Mench MM. Direct measurement of through-plane thermal conductivity and contact resistance in fuel cell materials. J Power Sources 2006;161:1106–15.
[19] Slade S, Campbell SA, Ralph TR, Walsh FC. Ionic conductivity of an extruded Nafion 1100 EW series of membranes. J Electrochem Soc 2002;149:A1556–64.
[20] Jung CY, Lee CS, Yi SC. Computational analysis of transport phenomena in proton exchange membrane for polymer electrolyte fuel cells. J Membrane Sci 2008;309:1–6.
[21] Bird RB, Stewart W, Lightfoot EN. Transport phenomena. New York: Wiley; 1973.
[22] Secanell M, Karan K, Suleman A, Djilali N. Optimal design of ultralow-platinum PEMFC anode electrodes. J Electrochem Soc 2008;155:B125–34.
[23] Sun W, Peppley BA, Karan K. An improved two-dimensional agglomerate cathode model to study the influence of catalyst layer structural parameters. Electrochim Acta 2005;50:3359–74.
[24] Shah AA, Kim GS, Sui PC, Harvey D. Transient non-isothermal model of a polymer electrolyte fuel cell. J Power Sources 2007;163:793–806.
[25] Springer TE, Zawodzinski TA, Gottesfeld S. Polymer electrolyte fuel cell model. J Electrochem Soc 1991;138:2334–42.
[26] Madhusudana RR, Bhattacharyya D, Rengaswamy R, Choudhury SR. A two-dimensional steady state model including the effect of liquid water for a PEM fuel cell cathode. J Power Sources 2007;173:375–93.